Atmos. Chem. Phys. Discuss., 13, 345–377, 2013
www.atmos-chem-phys-discuss.net/13/345/2013/
doi:10.5194/acpd-13-345-2013

Atmospheric Chemistry and Physics Discussions

Continuous atmospheric boundary layer observations in the coastal urban area of Barcelona, Spain

M. Pandolfi[1], G. Martucci[2], X. Querol[1], A. Alastuey[1], F. Wilsenack[3], S. Frey[4], C. D. O'Dowd[2], and M. Dall'Osto[1]

[1]Institute of Environmental Assessment and Water Research (IDAEA-CSIC), Barcelona, Spain
[2]School of Physics & Centre for Climate and Air Pollution Studies, Ryan Institute, National University of Ireland Galway, University Road, Galway, Ireland
[3]Wehrwissenschaftliches Institut für Schutztechnologien – ABC-Schutz, Germany
[4]Jenoptik Laser, Optik, Systeme GmbH, Germany

Received: 19 December 2012 – Accepted: 20 December 2012 – Published: 7 January 2013

Correspondence to: M. Pandolfi (marco.pandolfi@idaea.csic.es)

Published by Copernicus Publications on behalf of the European Geosciences Union.

Abstract

Continuous measurements of Surface Mixed Layer (SML), Decoupled Residual/Convective Layer (DRCL) and aerosol backscatter coefficient were performed within the Barcelona (NE Spain) boundary layer from September to October 2010 (30 days) in the framework of the SAPUSS (Solving Aerosol Problems Using Synergistic Strategies) field campaign. Two near-infrared ceilometers (Jenoptik CHM15K) vertically and horizontally-probing (only vertical profiles are discussed) were deployed during SAPUSS and compared with potential temperature profiles measured by daily radiosounding (midnight and midday) to interpret the boundary layer structure in the urban area of Barcelona. Ceilometer-based DRCL (1761 ± 363 m a.g.l.) averaged over the campaign duration were twice as high as the mean SML (904 ± 273 m a.g.l.) with a marked SML diurnal cycle. The overall agreement between the ceilometer-retrieved and radiosounding-based SML heights (R^2 = 0.8) revealed overestimation of the SML by the ceilometer (Δh = 145 ± 145 m). After separating the data in accordance with different atmospheric scenarios, the lowest SML (736 ± 183 m) and DRCL (1573 ± 428 m) were recorded during warm North African (NAF) advected air mass. By contrast, higher SML and DRCL were observed during stagnant regional (REG) (911 ± 234 m and 1769 ± 314 m, respectively) and cold Atlantic (ATL) (965 ± 222 m and 1878 ± 290 m, respectively) air masses. The SML during the NAF scenario frequently showed a flat upper boundary throughout the day because of strong winds from the Mediterranean Sea that limit the midday SML convective growth observed during ATL and REG scenarios. The mean backscatter coefficients were calculated at two selected heights as representative of middle and top SML portions, i.e. β_{500} = 0.59 ± 0.45 Mm^{-1} sr^{-1} and β_{800} = 0.87 ± 0.68 Mm^{-1} sr^{-1} at 500 m and 800 m a.g.l., respectively. The highest backscatter coefficients were observed during NAF (β_{500} = 0.77 ± 0.57 Mm^{-1} sr^{-1}) when compared with ATL (β_{500} = 0.51 ± 0.44 Mm^{-1} sr^{-1}) and REG (β_{500} = 0.64 ± 0.39 Mm^{-1} sr^{-1}).

The relationship between the vertical change in backscatter coefficient and atmospheric stability ($\partial\theta/\partial z$) was investigated in the first 3000 m a.g.l., demonstrating

ACPD
13, 345–377, 2013

a positive correlation between unstable conditions and enhanced backscatter and vice versa.

1 Introduction

The Planetary Boundary Layer (PBL) is the lowest part of the atmosphere that contains most atmospheric aerosols and humidity (Stull, 1988). A sound understanding of its main properties (such as height and temporal evolution) and of the factors affecting these properties is essential for meteorological forecasting, climate studies and air quality assessment (Gerbig et al., 2008; Monks et al., 2009). In fact, aerosols once emitted are confined within the PBL where they reside for a relatively long time and disperse or accumulate depending on the PBL characteristics such as height or wind fields. During the day the PBL undergoes a diurnal cycle with the deepest values around midday when convection is the main mixing force, yielding the shallowest values at night. During the night when convection is not the main mechanism, the PBL structure is largely influenced by surface friction due to vegetation, topography, or urban roughness (Barlow et al., 2011). The PBL depth is usually assessed in two ways: (i) by using in-situ vertical profiles of temperature, humidity or wind, and (ii) by employing the aerosols as tracers for laser-based backscatter profilers. The former method is a thermodynamic sounding which determines the top of the PBL through observation of temperature inversions, hydrolapse, or change in wind speed and/or wind direction (e.g. Holzworth, 1964, 1967). The latter method identifies the PBL heights by checking gradients in the aerosols concentrations and is usually applied by means of LIDARS/ceilometers (e.g. Martucci et al., 2010; Haeffelin et al., 2012). Other widely used remote sounding systems for PBL depth determination include sodar, rass and wind profiling radar. A number of methods have been employed to extract the PBL height from active optical methods, providing aerosol backscatter profiles. The decreasing laser backscatter from the aerosols at the interface (transition zone) between the PBL and the free troposphere is the essence of the method. The identified transition zone

Discussion Paper | Discussion Paper | Discussion Paper | Discussion Paper |

ACPD

13, 345–377, 2013

Continuous atmospheric boundary layer in Spain

M. Pandolfi et al.

is a proxy for temperature inversion. These methods involve the analysis of the first or second derivative of the backscatter or the logarithm of the backscatter profile (e.g. Flamant et al., 1997; Menut et al., 1999; Sicard et al., 2006; Martucci et al., 2007), THT (Temporal-Height-Tracking) technique (Martucci et al., 2010; Haeffelin et al., 2012), backscatter variance (e.g. Lammert and Bosenberg, 2006), among others. Methods based on the LIDAR determination of the PBL depth using aerosols as tracers may be adversely affected by the pre-processing of the data, gradient detection, and layer attribution, especially during morning or afternoon transitions or under stable atmospheric conditions (Haeffelin et al., 2012). Conversely, in well-mixed boundary layers, the largest change in the aerosol would match the top of the PBL with the free troposphere above, thus minimizing the uncertainty of retrieving the PBL top. Given the high spatial and temporal resolutions, (normally 15 m and 15 s), LIDARs and ceilometers have become increasingly important for PBL studies in the last few decades and are widely used in networks around the world and especially in Europe (e.g. Flentje et al., 2010; Pappalardo et al., 2004). Earlier studies have dealt with the determination of the evolution of the PBL by means of ground-based laser sensors at continental sites (e.g. Boers et al., 2000; Clothiaux et al., 2000; Matthias and Bösenberg, 2002; Kalb et al., 2004) or at coastal sites (e.g. Sicard et al., 2006, 2011; Matthias et al., 2004; Milroy et al., 2011). PBL heights at continental sites up to 2–3 km a.s.l. have been usually observed in summer (Matthias et al., 2004). Conversely, at sites closer to the coastline, no significant differences have been observed in the retrieved heights between summer and winter. De Tomasi et al. (2011) reported a case study of the PBL evolution over the coastal site of Lecce (Italy) during anticyclonic conditions with weak synoptic forcing. These authors attributed the reduction of the PBL height observed at noon to the sea breeze. Earlier measurements by LIDAR performed in Barcelona can be found for example in Sicard et al. (2006, 2011) and Pérez et al. (2004). In Barcelona the absence of a marked PBL annual cycle was related to the typical summer conditions of the Western Mediterranean Basin (WMB) characterised by weak pressure gradients and the development of breeze circulation patterns (Millán et al., 1997). These atmospheric conditions may prevent the vertical development of the PBL.

These distinctive characteristics of the WMB together with poor and irregular precipitations, frequent air mass advections from Africa (e.g. Millán et al., 1997; Rodríguez et al., 2001) cause the concentration, composition and vertical distribution of the atmospheric aerosols to be highly variable. Consequently, aerosol models and radiative transfer models still suffer from large uncertainties when applied to this region (e.g. Pay et al., 2012). Although a number of studies have focused on the evolution of the boundary layer at coastal sites in Europe (for example in Athens (Batchvarova and Gryning, 1998), Barcelona (Sicard et al., 2006, 2011), Marseille (Delbarre et al., 2005; Lemonsu et al., 2006), Naples (Boselli et al., 2009) and Rome (Mastrantonio et al., 1994), amongst others), only few works have addressed the problem of its diurnal evolution (Martano, 2002; Talbot et al., 2007; De Tomasi et al., 2011).

In this study, we analyse one month of continuous measurements of PBL height and optical properties over Barcelona (Spain), using the vertical-pointing 1064-nm wavelength CHM15K ceilometer within the framework of the SAPUSS (Solving Aerosol Problems Using Synergistic Strategies) project (Dall'Osto et al., 2012). The temporal evolution of the PBL height and aerosol backscatter at selected heights was studied for different atmospheric scenarios during the duration of the campaign. Three main atmospheric scenarios were defined: stagnant Regional (REG), warm African (NAF), and cold Atlantic (ATL). Ceilometer data together with radiosoundings were used to study the structure of PBL and its diurnal evolution for these detected scenarios. Aerosol backscatter coefficient and its relationship with unstable/stable atmospheric conditions are discussed.

ACPD
13, 345–377, 2013

2 Methodology

2.1 Measurement site

Ceilometer measurements were performed at the coastal site of Barcelona (BCN, Spain; 41° 23′ 24.01″ N, 2° 6′ 58.06″ E) from 20 September to 19 October 2010. The ceilometer was placed pointed vertically on the roof of a 8 m high building about 5 km from the sea in an urban background area. Barcelona and its satellite towns (with nearly 4.5 million inhabitants) occupy an 8 km wide strip between the Mediterranean Sea and the coastal mountain range. Moreover, several industrial zones, power plants, and highways are located in the area, making this region one of the most polluted in the WMB (Querol et al., 2008). Furthermore, during SAPUSS a second ceilometer was also deployed on the terrace of the Fabra observatory (41° 25′ 56″ N, 2° 07′ 27″ E; 500 m a.s.l.) in the coastal mountain range behind Barcelona pointing horizontally towards the sea. A future work will be dedicated to the horizontal ceilometer measurements. The main characteristics of the area under study and detailed information on the measurement sites and meteorology in the region during SAPUSS can be found in Dall'Osto et al. (2012).

2.2 Ceilometer

The vertical profiles of the LIDAR signals during the SAPUSS campaign were measured by the single-channel CHM15K (CHM) elastic LIDAR (ceilometer) manufactured by Jenoptik. The instrument is designed for continuous cloud base height determination and aerosol backscatter coefficient measurements during the day and night. The CHM uses a diode-pumped Nd:YAG solid state laser emitting low-energy laser pulses (8 µJ at 5.58 kHz) at the fundamental wavelength of 1064 nm. The instrument acquires signals in single photon counting mode thus increasing the signal-to-noise ratio from altitude where the concentration of aerosol is low. During the SAPUSS campaign, the ceilometer signals were collected every 30 s with a spatial (vertical) resolution of 15 m. The

ACPD
13, 345–377, 2013

CHM nominal spatial range is 30–15 000 m with 15 m corresponding to the first overlap point (Martucci et al., 2010). The overlap between emitter and receiver field of views is full at 1500 m (Martucci et al., 2010; Heese et al., 2010; Flentje et al., 2010; Milroy et al., 2011). However, because of the steep slope of the overlap function, the region above 500 m has > 60 % overlap (Martucci et al., 2010). Moreover, as shown by Milroy et al. (2011) during a multi-sensor comparative study performed at Mace Head (Ireland), the CHM15K signal clearly detects aerosol layers and the PBL internal structure at heights > 500 m. Mainly because of the low-power of its laser pulses, the ceilometer has been compared with more powerful LIDARs designed for tropospheric aerosol studies (Heese et al., 2010; Freudenthaler et al., 2010; Tsaknakis et al., 2011, Haeffelin et al., 2012; Milroy et al., 2011). These comparisons have also been performed to determine the altitude at which the ceilometers are able to detect the aerosols with a signal-to-noise ratio > 1. Heese et al. (2010) found that the CHM15K can detect aerosol backscatter with signal-to-noise ratio (SNR) > 1 in the boundary layer and up to ∼ 4 km during daytime and up to 9 km during the night. Moreover, Martucci et al. (2010) compared the CHM15k ceilometer with another commercial ceilometer from Vaisala (model CL31) and concluded that the CHM15K has better retrieval skills of the cloud base and a higher sensitivity to aerosols below the cloud base.

2.2.1 Aerosol backscatter coefficients from ceilometers

Knowledge of the maximum height with SNR > 1 is of paramount importance for the correct retrieval of the backscatter coefficient vertical profiles at different times of the day. The radiation collected by the ceilometer is in fact backscattered from aerosols and molecules and the discrimination of the aerosol contribution requires measurements of the molecular backscatter with SNR > 1 at altitudes where aerosols are not present (Klett, 1981; Ferguson and Stephens, 1983).

In this work the aerosol backscatter coefficients were retrieved at two selected heights, i.e. at 500 m and 800 m a.g.l. for the entire SAPUSS campaign. The backscatter coefficients at these heights are referred to as β_{500} and β_{800} hereafter. Moreover,

ACPD
13, 345–377, 2013

vertical profiles of aerosol backscatter coefficients were retrieved for each day during SAPUSS, integrating the ceilometer signals over 30 min between 12:00 and 12:30 UTC.

2.2.2 Determination of SML and DRCL heights by ceilometer

The PBL height and vertical structure above Barcelona was retrieved with standard 30-s and 15-m temporal and vertical resolution, respectively, by applying the Temporal-Height-Tracking (THT, Martucci et al., 2010; Haeffelin et al., 2012) algorithm to the LIDAR returns from the CHM15K. The THT is 1-D (spatial) gradient and time-constrained technique to retrieve the PBL structure. Two layers are retrieved by the THT at each time step: a Surface Mixed Layer (SML, lower layer), which is a proxy for temperature inversion, and a Decoupled Residual/Convective Layer (DRCL, upper layer) above which is the free troposphere. The two layers are calculated by applying the THT to an m-by-n matrix (m = number of range gates; n = number of profiles) of attenuated backscatter coefficients, i.e. the natural logarithm of the background-power-range corrected LIDAR return. The THT selects the first gradient (SML) along the time-averaged profile with high SNR (averaging interval duration, e.g., $T_{\text{interv}} = 10$ min). The time-averaged profile provides the reference height (H_{ref}) for the first ($t = 1$) and the successive ($t > 1$) SML detections. A vertical window centred in H_{ref} with amplitude normally set to $H_{\text{ref}} \pm 150$ m constrains the SML detection at time steps t, $t+1$, $t+2$, ... and so on until the end of the reference interval T_{interv}. New reference heights are calculated at the beginning of each block of $N \cdot T_{\text{interv}}$ ($N = 1$, ...) until the end of the dataset. The same procedure is repeated for the upper DRCL. Data from the ceilometer were carefully cloud screened to avoid any bias due to cloud scattering.

2.3 Radiosoundings

Vertical profiles of temperature, pressure, relative humidity, wind speed and velocity were obtained twice a day from radiosondes (model Vaisala RS92-SGP) launched at

ACPD
13, 345–377, 2013

00:00 UTC and 12:00 UTC from a co-located radiosounding system run by the Physics Department of the University of Barcelona. The launching site was about 50 m from the location of the ceilometer.

2.3.1 SML height determination by radiosoundings

For the determination of the SML heights from radiosonde data during SAPUSS, we used the simple parcel method described by Holzworth (Holzworth, 1964). With this method the SML height is taken as the equilibrium level of an air parcel with the potential temperature (θ) calculated at ground level. The potential temperature of an air parcel at pressure P is the temperature that the parcel would acquire if it is adiabatically brought to a standard reference pressure P_0 (usually 1000 mbar) and is calculated from pressure and temperature data as follows:

$$\theta = T \times \left(\frac{1000}{P}\right)^{0.286} \tag{1}$$

where T [K] is the actual temperature, P [mbar] is the pressure of the air parcel and 0.286 is the ratio between the gas constant of air (R) and the specific heat capacity at a constant pressure (c_p).

The parcel method allows us to determine the PBL heights in the case of marked inversions which are usually observed during the day but which may also characterise the nocturnal atmosphere.

2.4 Other measurements

Hourly ground ambient temperature, relative humidity, wind speed and direction data were obtained with a meteorological station placed at the Barcelona urban background (UB) measurement site described in Reche et al. (2011) and Dall'Osto et al. (2012) and located about 400 m from the ceilometer. Particulate matter (PM) concentrations were obtained during SAPUSS by means of GRIMM optical counters (model 1107) at the UB site. Aerosol Optical Depth (AOD) data were obtained from a sunphotometer operating within AERONET (the AERosol Robotic NETwork of ground-based sun- and sky-scanning radiometers; Holben et al., 1998) and located about 50 m from the ceilometer. The AERONET cloud screened Level2 data were used in this work. Moreover, data from the sunphotometer were used to retrieve the aerosol Ångström exponents (*å*), which are a proxy for aerosol size. An aerosol distribution dominated by coarser particles is characterised by values lower than 1 whereas larger *å* (higher than 2) indicate that the scattering is dominated by submicron particles (Schuster et al., 2006).

2.5 Atmospheric scenarios observed during SAPUSS

During the SAPUSS campaign three different atmospheric scenarios, namely Regional (REG), Atlantic (ATL), and African (NAF) were observed. These scenarios are not uncommon in the Western Mediterranean in summer (i.e. Millan et al., 2000; Pey et al., 2010; Pandolfi et al., 2011). A brief description of their main characteristics is given below whereas the detailed meteorological picture during SAPUSS and the description of tools used for meteorological analysis are provided in the overview of the SAPUSS campaign (Dall'Osto et al., 2012).

The REG scenario typically develops under meteorological conditions characterised by insignificant air mass circulation at the synoptic scale, thus occasionally favouring the accumulation of pollutants. The ATL scenario represents advections from the Atlantic Ocean associated with cold fronts crossing the Iberian Peninsula (IP). This scenario leads to the renovation of accumulated pollution in aged air masses with a consequent reduction in pollutant concentrations. Finally, the NAF scenario identifies the days characterised by air masses from Africa. During the campaign, a total of 9, 7, and 6 days were identified as REG, ATL and NAF, respectively. Moreover, the NAF days were further classified as NAF_E and NAF_W. NAF_E (3 days) is characterised by air mass types proceeding from the Sahara and arriving in Barcelona from the E, i.e. from the Mediterranean Sea, whereas NAF_W (3 days) is marked by air masses proceeding

ACPD
13, 345–377, 2013

from the Tropical Atlantic Ocean and arriving in Barcelona from the SW after crossing the Iberian Peninsula (Dall'Osto et al., 2012).

3 Results

This section is concerned with the mean characteristics and daily evolutions of SML, DRCL, β_{500} and β_{800} measured over Barcelona during SAPUSS. Ground meteorological data and ground PM_1 concentrations are presented and correlated with the measured aerosol optical properties. The mean values and diurnal cycles of these variables for the entire SAPUSS campaign (ALL) and for the REG, ATL and NAF scenarios are presented in Table 1 and Fig. 1. Table 1 also gives the mean AOD and Ångström exponents ($\mathring{a}$) observed during the campaign.

3.1 Mean characteristics during SAPUSS

The mean ceilometer SML and DRCL heights over the whole SAPUSS campaign (ALL, cf. Table 1) are 904 ± 273 m a.g.l. and 1761 ± 363 m a.g.l., respectively. This is in agreement with Sicard et al. (2011), who reported for September and October a mean mixing layer height of around 750–1200 m a.g.l. based on three-year lidar measurements. Mean β_{500} and β_{800} during SAPUSS are $0.59 \pm 0.45\,\mathrm{Mm^{-1}\,sr^{-1}}$ and $0.87 \pm 0.68\,\mathrm{Mm^{-1}\,sr^{-1}}$, respectively, the latter being consistent with the mean backscatter at 900 m reported by Sicard et al. (2011) for summer. The mean AOD and $\mathring{a}$ measured during SAPUSS are around 0.08 ± 0.10 and 1.2 ± 0.4, respectively, close to the mean values reported for these parameters in Barcelona for the summer period (Pandolfi et al., 2011; Sicard et al., 2011). The mean ground PM_1 ($12.6 \pm 4.4\,\mu\mathrm{g\,m^{-3}}$) concentrations are lower compared with the mean PM_1 concentrations (around $17\,\mu\mathrm{g\,m^{-3}}$) registered in Barcelona during September and October for the period 2003–2005 (Pey et al., 2010) and similar to the mean PM_1 for the 2008–2011 period. The general tendency of the fine PM mass to decrease over the last years in the WMB (Cusack et al.,

ACPD
13, 345–377, 2013

2012) probably accounted for the lower PM_1 concentrations during SAPUSS when compared with previous years.

3.1.1 Mean diurnal cycles during SAPUSS

On average, during SAPUSS the SML height show a diurnal cycle (ALL; Fig. 1) with lower heights measured at night/early morning (~ 800 m around 18:00–06:00 UTC) increasing by around 50 % at midday (~ 1200 m around 12:00–14:00 UTC) when the surface temperature is at its maximum (Fig. 1). Thus, the increasing convective activity during the warmest hours of the day caused the increase in SML depth at midday.

Opposite diurnal cycles are observed for β_{500} and β_{800}, which show the highest values at night (0.77 $Mm^{-1} sr^{-1}$ and 1.07 $Mm^{-1} sr^{-1}$, respectively, around 18:00–06:00 UTC) and the lowest (0.36 $Mm^{-1} sr^{-1}$ and 0.67 $Mm^{-1} sr^{-1}$, respectively) around midday (cf. ALL in Fig. 1). The difference in backscatter between day and night was probably due to the increase in relative humidity at night (cf. RH in Fig. 1) leading to a significant hygroscopic growth of aerosols. Radiosonde data were used to calculate the relative difference (%) in RH between night (00:00 UTC) and day (12:00 UTC) at 500 m and 800 m a.g.l. during SAPUSS. The RH relative differences were then compared with the relative differences (%) in β_{500} and β_{800} between night and day. Figure 2 gives the results of the intercomparison showing that the variations in backscatter coefficients between night and day are highly correlated with the corresponding variations in RH. Thus RH is an important parameter contributing to the variation in aerosol backscatters. Moreover, the lower SML height and dispersion at night (lower wind speed, cf. Fig. 1) compared with daytime favour the accumulation of particles (higher PM_1 concentrations at night, cf. Fig. 1) which also contribute to the relative increase in backscatter at night.

3.2 Mean characteristics during ATL, REG and NAF

Important differences are observed in the variables reported in Table 1 for the three scenarios (REG, ATL, NAF) during SAPUSS. The highest mean SML and DRCL heights

ACPD
13, 345–377, 2013

are observed for the ATL scenario at around 965 ± 222 m and 1878 ± 290 m a.g.l., respectively (Table 1). These heights are slightly higher (around 6 %) than the mean SML and DRCL observed during the REG scenario at 911 ± 234 m and 1769 ± 314 m a.g.l., respectively. Nevertheless, under ATL the mean β_{500} ($0.51 \pm 0.44\,\mathrm{Mm^{-1}\,sr^{-1}}$), β_{800} ($0.78 \pm 0.72\,\mathrm{Mm^{-1}\,sr^{-1}}$), PM_1 ($9.8 \pm 1.1\,\mu\mathrm{g\,m^{-3}}$), AOD (0.03 ± 0.02), and the Angstrom exponent (1.3 ± 0.3) are lower by, respectively 20 %, 24 %, 40 %, 60 % and 14 % compared with REG (Table 1). Lower fine aerosol concentrations and AOD during ATL were due to the cleansing effect of the Atlantic advections that reduce the concentration of fine aerosol in the atmosphere. At the same time, the accumulation of pollutants was favoured by the REG episode, and the concentrations of PM_1 reach $16.3 \pm 5.3\,\mu\mathrm{g\,m^{-3}}$. The low concentrations of fine PM for the ATL scenario led to $\mathring{a}$ coefficients higher than those for REG, indicating larger concentrations of coarse particles during ATL. The low relative humidity measured during ATL (Table 1) also contributed to the low β_{500} and β_{800} during this scenario. Figure SI-1 (in Supplement) shows that the mean RH during ATL is the lowest during SAPUSS at all altitudes, being about 20 % lower in the first one kilometre of height with respect to REG.

The lowest mean daily SML and DRCL were detected during the NAF scenario at altitudes around 736 ± 183 m a.g.l. and 1573 ± 428 m a.g.l., respectively (Table 1). The SML and DRCL heights during NAF are, respectively 25 % and 16 % lower than for the ATL scenario. The mean daily SML during NAF ranged between 609 ± 128 m on 8 October and 798 ± 106 m on 7 October, whereas the minimum and maximum mean daily SML heights during ATL were 895 ± 209 m (on 26 September) and 1022 ± 205 m (on 28 September), respectively. Thus, significant differences are observed between the NAF scenario and the ATL and REG scenarios in terms of the SML and DRCL heights. The NAF scenario also registered the highest mean β_{500} ($0.77 \pm 0.57\,\mathrm{Mm^{-1}\,sr^{-1}}$) and β_{800} ($1.14 \pm 0.72\,\mathrm{Mm^{-1}\,sr^{-1}}$) measured during the campaign. The calculated β_{500} and β_{800} under NAF were, respectively, 20 % and 15 % higher than under REG and 50 % and 46 %, respectively, higher compared with ATL. The main reason for the high β_{500} and β_{800} measured during NAF was the transport of dust from Africa, which increased

ACPD
13, 345–377, 2013

the aerosol backscatter. As shown in Table 1, the highest mean column integrated AOD (0.24±0.17) and the lowest mean $\mathring{a}$ (0.7±0.6) were observed during the NAF scenario, suggesting transport of coarser aerosols from North Africa. Figure SI-2 in Supplement highlights the relationship between AOD and simultaneous β_{500} and β_{800} by levels of Ångström exponents, showing that the lowest $\mathring{a}$ were observed during NAF. These were especially low (< 0.12) during a dust transport event detected on 7 October, leading to the highest AOD (> 0.3) during SAPUSS. Nevertheless, the β_{500} and β_{800} were relatively low during the event, suggesting transport of dust at higher altitudes over Barcelona. After excluding the data collected on 7 October the mean AOD, $\mathring{a}$, β_{500} and β_{800} during NAF were, respectively, 0.11 ± 0.04, 1.0 ± 0.3, 0.80 ± 0.59 $\mathrm{M\,m^{-1}\,sr^{-1}}$, and 1.09 ± 0.71 $\mathrm{M\,m^{-1}\,sr^{-1}}$, strongly suggesting coarse aerosols within the PBL during the whole NAF scenario. Moreover, the presence of dust transported from Africa under NAF is also evidenced in Fig. SI-1, which shows the multiple-peak structure of the mean aerosol backscatter vertical profile.

Moreover, the low SML and the high RH observed under NAF (around 75 % at ground, cf. Table 1) may also have contributed to the high backscatter observed under NAF. In fact, Fig. SI-1 shows that mean RH during NAF is the highest during SAPUSS at all altitudes, being on average 47 % higher in the first one kilometre compared with ATL.

3.2.1 Mean diurnal cycles during ATL, REG and NAF

The most striking differences among the three scenarios in terms of diurnal cycles are observed for SML, β_{500} and β_{800} (Fig. 1). Figure 1 shows that the mean SML during NAF has a flat structure between approximately 11:00 and 16:00 UTC compared with the ATL and REG scenarios, which by contrast show clear SML maxima around midday. The flat SML structure under NAF is present despite the high surface temperatures at midday under NAF with respect to REG and ATL (cf. Fig. 1). The mean SML heights (±1 standard deviation) between 11:00 and 16:00 UTC are 1133±354 m, 1107±313 m,

ACPD
13, 345–377, 2013

Title Page
Abstract | Introduction
Conclusions | References
Tables | Figures
Back | Close
Full Screen / Esc
Printer-friendly Version
Interactive Discussion

and 916 ± 168 m for ATL, REG and NAF, respectively, with the lowest standard deviation around 18 % observed for the NAF scenario compared with ATL (31 %) or REG (28 %).

The mean diurnal cycles of β_{500} and β_{800} during ATL, REG and NAF are fairly similar, showing higher values at night and minima during daytime. However, the diurnal cycles of backscatter under NAF also shows the presence of multiple peaks due to transported dust from Africa.

Finally, the importance of RH variation in determining the scattering properties of aerosols can be assessed here by looking at the diurnal cycles of β_{500}, β_{800}, PM_1 and RH under ATL (Fig. 1). During ATL both β_{500} and β_{800} show clear diurnal cycles whereas the PM_1 concentrations show no diurnal cycle, being fairly constant throughout the 24 h. Conversely, under the NAF and REG scenarios, variations in the diurnal cycles in PM_1 concentrations and β_{500} and β_{800} are observed. Figure 1 shows that the ground wind velocity during ATL was fairly high and constant throughout the day. This is probably the most important variable determining the low daily variability in PM_1 concentrations. Conversely, the RH, for which a clear diurnal cycle is observed under ATL, is the main parameter driving the diurnal cycles of aerosol backscatter (cf. Fig. 1).

3.3 SML height: ceilometer vs. radiosonde

Figure 3 shows the relationship between the SML heights estimated from radiosoundings and ceilometer data at 12:00 UTC for the whole SAPUSS campaign and for each scenario. A good correlation ($R^2 = 0.80$; p-value < 0.05) is observed between the retrieved SML heights during the whole SAPUSS campaign (ALL). On average, the SML heights from radiosoundings were lower than those from the ceilometer by around 145 ± 145 m (error calculated as one standard deviation of the data). Recently, Haeffelin et al. (2012) showed that LIDAR/ceilometers tend to overestimate the mixing heights compared with radiosoundings. The deviations we observed were of the same sign and range of the deviations reported by Haeffelin et al. Good correlations are also observed specifically for each scenario, with coefficients of determination R^2 ranging from 0.75 (REG; p-value < 0.1) to 0.96 (NAF; p-value < 0.4). On average, the highest

ACPD
13, 345–377, 2013

differences are detected for the REG and ATL scenarios with values around 166±125 m and 249 ± 43 m, respectively, whereas during the NAF scenario the difference is small and slightly negative (−42 ± 41 m).

4 Discussion

From the above it follows that the lowest mean SML and DRCL heights during SAPUSS were detected during the NAF scenario. The shallow SML during NAF was also measured by radiosoundings which detected mean SML heights at 953 ± 138 m, 925±183 m, and 800±206 m for ATL, REG and NAF, respectively. During NAF, the SML also showed a flat structure around midday when the REG and ATL SMLs yielded maxima. These distinctive characteristics of the lower atmosphere during NAF were probably due to the concomitance of different factors. The low SML and DRCL may have been caused by a pushing-down effect of the warm overhanging African air masses which changed the temperature profile thus lowering the inversion. The compression of the SML favoured the transport of the Saharan dust down towards the surface layers by dry deposition, resulting in the increase in β_{500} and β_{800}. Alastuey et al. (2005) reported a significant decrease in the marine boundary layer at Izaña (South of Spain) during an intense Saharan dust outbreak with the overhanging African air masses lowering the marine PBL up to 400 m. Similarly, in Barcelona Pérez et al. (2004) reported a low SML height, ranging between about 300 m and 440 m during an intense Saharan dust outbreak.

The flat structure observed for SML around midday during NAF was probably due to the increase in the mean wind velocities within the SML preventing the vertical development of the SML. This was observed on three out of the six NAF days. As described above, the NAF days were divided into two main categories, namely NAF_E (7–8–9 October 2010) and NAF_W (22–23 September and 3 October 2010) (Dall'Osto et al., 2012). Figure 4 shows the SML and DRCL diurnal cycles from the ceilometer and the SML heights from the radiosoundings at 12:00 GMT for the NAF_W days (Fig. 4a) and the NAF_E days (Fig. 4b). During the NAF_W days the SML shows a certain convective growth around midday. Nevertheless, the SML growth under NAF_W was not as strong as during ATL and REG scenarios because of the overhanging African air masses. Conversely, a flat SML structure throughout the 24 h was observed under the NAF_E days probably due to the strong winds blowing continuously from the Mediterranean Sea and preventing the vertical development of the SML. In fact, Fig. 4 shows that the mean wind direction (wd) and speed (ws) within the first kilometre a.g.l. during NAF_W are around 214 ± 39 degrees (South-West) and $3.6 \pm 1.7\,\mathrm{m\,s^{-1}}$, respectively, whereas during NAF_E the mean wd and ws are 73 ± 17 degrees (East) and $6.9 \pm 0.9\,\mathrm{m\,s^{-1}}$, respectively. The low standard deviations indicated relatively constant vertical profiles of wind speed and direction during NAF_W and NAF_E. The mean wind speed within the first kilometre during NAF_E doubled the mean wind velocity under NAF_W, REG ($3.2 \pm 1.2\,\mathrm{m\,s^{-1}}$) and ATL ($3.8 \pm 1.5\,\mathrm{m\,s^{-1}}$) days, probably preventing the SML from developing under NAF_E. Reduced growth of PBL caused by strong winds from the sea have been reported at other coastal sites (i.e. De Tomasi et al., 2011).

The presence of African air masses above Barcelona during NAF could be one of the reasons for the good agreement observed between radiosondes and ceilometer in estimating the SML heights during NAF (cf. Fig. 3). The 5-day back-trajectories ending in Barcelona at 12:00 UTC and calculated for the NAF days (two examples are shown in Fig. SI-3 in Supplement) display differential advections of air masses at different heights. The air mass ending at 1000 m a.g.l. clearly came from Africa. This differential advection may have caused an abrupt change in physical and thermodynamic properties of SML, thus minimizing the differences typically observed between ceilometer and radiosondes in estimating the SML height. Conversely, during the ATL scenario the air masses had the same origin at the altitudes considered (cf. Fig. SI-4) and the largest difference between the SML heights can be observed.

Figure 3 shows that the changes in the thermodynamic state of the atmosphere at the top of the SML are closely correlated with the variations in the aerosol load. The correlation is studied in greater depth here by comparing the potential temperature and

ACPD
13, 345–377, 2013

aerosol backscatter vertical profiles from 500 m up to 3000 m a.g.l. This analysis seeks to show how the unstable, stable or neutral atmospheric conditions of the atmosphere alter the distribution of aerosol backscatter with height. Fourteen vertical profiles of aerosol backscatter integrated between 12:00 and 12:30 UTC (no clouds included) were selected and compared with the potential temperature profiles from radiosondes launched at 12:00 UTC. The 14 profile pairs were interpolated to a vertical resolution of 30 m and were averaged to obtain one pair of mean aerosol backscatter and potential temperature vertical profiles. Figure 5a shows the relationship between the first derivatives with height of the mean aerosol backscatter and potential temperature profiles, ranging between 500 m and 3000 m a.g.l. with $\Delta z = 30$ m. Figure 5b is calculated by averaging the first derivatives every 200 m ($\Delta z = 200$) and error bars in Fig. 5b indicate ±1 standard deviation of the means. Figure 5c, d is similar to Figure 5a, b, respectively, and was obtained by using a subset of 4 profile pairs which showed different characteristics as described below. The NAF days were excluded from this analysis because the gradients of the backscatter coefficient in the presence of aerosol layers of different origin were strong enough to impair the backscatter-temperature relationship. The mean vertical profiles of backscatter, potential temperature and relative humidity calculated by averaging the 14 profiles are shown in Fig. SI-5 in Supplement. Figure 5a, b shows that the backscatter coefficient increases with height ($\mathrm{d}\beta/\mathrm{d}z > 0$) at altitudes (between about 500 and 900 m) where θ is fairly constant or increases slightly with height ($\mathrm{d}\vartheta/\mathrm{d}z \sim 0$). This first altitude range represents the mean SML depth. In this range, convection rapidly mixes the atmosphere with the result that θ is fairly constant with height and the atmosphere is characterised by neutral stability. Above ~ 1000 m and up to ~ 1700 m the backscatter coefficient decreases with height ($\mathrm{d}\beta/\mathrm{d}z > 0$), showing a slightly negative slope around 900–1100 m, which becomes steeper with increasing height up to 1500–1700 m. This altitude range represents the atmospheric region between the top of SML and the DRCL. Conversely, the potential temperature increases with height from 1000 m up to 1700 m ($\mathrm{d}\vartheta/\mathrm{d}z > 0$), showing steeper positive slopes with increasing altitudes. These conditions give rise to stable

Discussion Paper | Discussion Paper | Discussion Paper | Discussion Paper |

ACPD
13, 345–377, 2013

Continuous atmospheric boundary layer in Spain

M. Pandolfi et al.

stratified conditions with suppressed vertical motions. The increasing and decreasing trend of aerosol backscatter coefficient as a function of the potential temperature between 500 m and 1700 m is highlighted by the yellow area in Fig. 5b. From ∼ 1700 m up to 3000 m the backscatter coefficient shows a very small negative derivative, indicating a gentle decrease in aerosol backscatter with height in the free troposphere. By contrast, at these heights the potential temperature increases showing steeper slopes with altitude ($d\vartheta/dz > 0$). The behaviour of both variables in the free troposphere is highlighted by the blue area in Fig. 5b.

The anticorrelation/correlation reported in Fig. 5 changes with height, allowing for the identification of SML, residual layer (RL), DRCL, and free troposphere (FT).

Figure 5c, d was obtained by using a subset of 4 profile pairs when the lower atmosphere showed a certain degree of instability ($d\theta/dz < 0$) up to about 600 m a.g.l. Nevertheless, the backscatter behaves in the same way as it does under neutral conditions and increases with height ($d\beta/dz > 0$). The observed increase of aerosol backscatter within the SML at midday irrespective of the thermodynamic states of the atmosphere is probably due to the increase with height in relative humidity within the SML. Figure 6a, b shows the relationship between the first derivatives of backscatter coefficient and relative humidity profiles as a function of height. Figure 6a, b shows that both backscatter and relative humidity increase with height between 500 m and 900 m (within the SML) and decrease with height starting from 900 m. In the free troposphere (blue coloured area) the backscatter decreases only slightly with height, with the RH showing steeper slopes with respect to backscatter.

Finally, the mean slopes of the LIDAR backscatter and potential temperature profiles at the top of the SML during NAF were $-0.038 \pm 0.007\,\mathrm{Mm^{-1}\,sr^{-1}\,m^{-1}}$ and $+0.018 \pm 0.007\,\mathrm{K\,m^{-1}}$, respectively, at 12:00 UTC. By comparing these values with Fig. 5, we conclude that an abrupt change is observed between the top of SML and the free troposphere during NAF. The potential temperature first derivative during the NAF scenario was in the upper range of values (cf. Fig. 5a), whereas for the backscatter the first derivatives were much higher and were considered as outliers. These values corroborate the hypothesis that the differential advection accounts for the good agreement between the SML heights retrieved from the ceilometer and the radiosoundings during NAF.

In summary, this study conducted in Barcelona during the SAPUSS project revealed the most salient features of the PBL:

- PBL maximum height and daily variations (DV) were strongly dependent on air mass types, ranging from the highest PBL-strongest DV (ATL) to the lowest PBL-weakest DV (NAF).
- Aerosol backscattering coefficients (BSC) were highly variable, with the highest values influenced by both African dust intrusions (NAF) and regional anthropogenic pollution (REG).
- In the portion of the atmosphere (SML) characterised by neutral thermodynamic stability conditions ($d\theta/dz \sim 0$) at midday, the BSC increased in parallel with RH with altitude. By contrast, under the stable stratified conditions ($d\theta/dz > 0$) above the SML, BSC decreased with falling RH with height. The increase in BSC with altitude was also detected under unstable atmospheric conditions ($d\theta/dz < 0$).

The measurements presented in this study yield valuable insights into the spatial and temporal distribution of the PBL characteristics and aerosol optical properties in a coastal Mediterranean area.

Supplementary material related to this article is available online at: http://www.atmos-chem-phys-discuss.net/13/345/2013/acpd-13-345-2013-supplement.pdf.

Acknowledgement. This study was supported by the Ministry of Science and Innovation (CARIATI CGL2008-06294/CLI, GRACCIE CSD2007-00067), the project number 254773, SAPUSS – Solving Aerosol Problems Using Synergistic Strategies (Marie Curie Actions), the

Generalitat de Catalunya (2009 SGR8). The authors gratefully acknowledge the NOAA Air Resources Laboratory (ARL) for the provision of the HYSPLIT transport and dispersion model and/or READY website (http://www.arl.noaa.gov/ready.html) used in this publication. Thanks are also due to José Ma. Baldasano and staff for their help in establishing and maintaining the Barcelona AERONET measurement site. The authors wish to thank the Catalan Meteorological Service for providing the BCN radiosounding data. The authors wish to thank D. C. Carslaw and K. Ropkins for providing the Openair software used in this paper (Carslaw and Ropkins, 2012; Carslaw, 2012).

References

Alastuey, A., Querol, X., Castillo, S., Escudero, M., Avila, A., Cuevas, E., Torres, C., Romero, P. M., Exposito, F., García, O., Diaz, J. P., Van Dingenen, R., and Putaud, J. P.: Characterisation of TSP and $PM_{2.5}$ at Izaña and Sta. Cruz de Tenerife (Canary Islands, Spain) during a Saharan Dust Episode (July 2002), Atmos. Environ., 39, 4715–4728, 2005.

Barlow, J. F., Dunbar, T. M., Nemitz, E. G., Wood, C. R., Gallagher, M. W., Davies, F., O'Connor, E., and Harrison, R. M.: Boundary layer dynamics over London, UK, as observed using Doppler lidar during REPARTEE-II, Atmos. Chem. Phys., 11, 2111–2125, doi:10.5194/acp-11-2111-2011, 2011.

Batchvarova, E. and Gryning, S. E.: Wind climatology, atmospheric turbulence and internal boundary-layer development in Athens during the MEDCAPHOT-TRACE experiment, Atmos. Environ., 32, 2055–2069, 1998.

Boers, R., Russchenberg, H., Erkelens, J., and Venema, V.: Ground-based remote sensing of stratocumulus properties during CLARA, J. Appl. Meteor., 39, 169–181, 2000.

Boselli, A., Armenante, M., D'Avino, L., D'Isidoro, M., Pisani, G., Spinelli, N., and Wang, X.: Atmospheric aerosol characterization over Naples during 2000–2003 EARLINET project: planetary boundary-layer evolution and layering, Bound.-Layer Meteorol., 132, 151–165, 2009.

Carslaw, D. C.: The openair manual – open-source tools for analysing air pollution data, Manual for version 0.7-0, King's College London, 2012.

Carslaw, D. C. and Ropkins, K.: openair – an R package for air quality data analysis, Environ. Modell. Softw., 27–28, 52–61, 2012.

Clothiaux, E. E., Ackerman, T. P., Mace, G. C., Moran, K. P., Marchand, R. T., Miller, M. A., and Martner, B. E.: Objective determination of cloud heights and radar reflectivities using a combination of active remote sensors at the ARM CART site, J. Appl. Meteor., 39, 645–665, 2000.

Cusack, M., Alastuey, A., Pérez, N., Pey, J., and Querol, X.: Trends of particulate matter ($PM_{2.5}$) and chemical composition at a regional background site in the Western Mediterranean over the last nine years (2002–2010), Atmos. Chem. Phys., 12, 8341–8357, doi:10.5194/acp-12-8341-2012, 2012.

Dall'Osto, M., Querol, X., Alastuey, A., Minguillon, M. C., Alier, M., Amato, F., Brines, M., Cusak, M., Grimalt, J. O., Karanasiou, A., Moreno, T., Pandolfi, M., Pey, J., Reche, C., Ripoll, A., Tauler, R., Van Drooge, B. L., Viana, M., Harrison, R. M., Gietl, J., Beddows, D., Bloss, W., O'Dowd, C., Ceburnis, D., Martucci, G., Ng, S., Worsnop, D., Wenger, J., Mc Gillcuddy, E., Sudou, J., Healy, R., Lucarelli, F., Nava, S., Jimenez, J. L., Gomez Moreno, F., Artinano, B., Prevot, A. S. H., Pfaffenberger, L., Frey, S., Wilsenack, F., Casabona, D., Jiménez-Guerrero, P., Gross, D., and Cotz, N.: Presenting SAPUSS: solving aerosol problem by using synergistic strategies at Barcelona, Spain, Atmos. Chem. Phys. Discuss., 12, 18741–18815, doi:10.5194/acpd-12-18741-2012, 2012.

Delbarre, H., Augustin, P., Saïd, F., Campistron, B., Benech, B., Lohou, F., Puygrenier, V., Moppert, C., Cousin, F., Freville, P., and Frejafon, E.: Ground-based remote sensing observation of the complex behaviour of the Marseille boundary layer during ESCOMPTE, Atmos. Res., 74, 403–433, 2005.

De Tomasi, F., Miglietta, M., and Perrone, M. R.: The growth of the planetary boundary layer at a coastal site: a case study, Bound.-Layer Meteorol., 139, 521–554, 2011.

Ferguson, J. A. and Stephens, D. H.: Algorithm for inverting lidar returns, Appl. Opt., 22, 3673–3675, 1983.

Flamant, C., Pelon, J., Flamant, P. H., and Durand, P.: Lidar determination of the entrainment zone thickness at the top of the unstable marine atmospheric boundary layer, Bound.-Layer Meteorol., 83, 247–284, 1997.

Flentje, H., Heese, B., Reichardt, J., and Thomas, W.: Aerosol profiling using the ceilometer network of the German Meteorological Service, Atmos. Meas. Tech. Discuss., 3, 3643–3673, doi:10.5194/amtd-3-3643-2010, 2010.

Freudenthaler, V., Gross, S., Engelmann, R., Mattis, I., Wandinger, U., Pappalardo, G., Amodeo, A., Giunta, A., D'Amico, G., Chaikovsky, A., Osipenko, F., Slesar, A., Nicolae, D.,

Belegante, L., Talianu, C., Serikov, 5 I., Linne, H., Jansen, F., Wilson, K., de Graaf, M., Apituley, A., Trickl, T., Giehl, H., and Adam, M.: EARLI09 –Direct intercomparison of eleven EARLINET lidar, 25th International Laser Radar Conference (ILRC), St. Petersburg, Russia, S7O–05, p. 61, available at: http://ilrc25.iao.ru/conference/program, 2010.
Gerbig, C., Körner, S., and Lin, J. C.: Vertical mixing in atmospheric tracer transport models: error characterization and propagation, Atmos. Chem. Phys., 8, 591–602, doi:10.5194/acp-8-591-2008, 2008.
Haeffelin, M., Angelini, F., Morille, Y., Martucci, G., Frey, S., Gobbi, G. P., Lolli, S., O'Dowd, C. D., Sauvage, L., Xueref-Rémy, I., Wastine, B., and Feist, D. G.: Evolution of mixing-height retrievals from automatic profiling lidars and ceilometers in view of future integrated networks in Europe, Bound.-Layer Meteorol., 143, 49–75, 2012.
Heese, B., Flentje, H., Althausen, D., Ansmann, A., and Frey, S.: Ceilometer lidar comparison: backscatter coefficient retrieval and signal-to-noise ratio determination, Atmos. Meas. Tech., 3, 1763–1770, doi:10.5194/amt-3-1763-2010, 2010.
Holben, B. N., Eck, T. F., Slutsker, I., Tanre, D., Buis, J. P., Setzer, A., Vermote, E., Reagan, J. A., Kaufman, Y. J., Nakajima, T., Lavenu, F., Jankowiak, I., and Smirnov, A.: AERONET – a federated instrument network and data archive for aerosol characterization, Remote Sens. Environ., 66, 1–16, 1998.
Holzworth, C. G.: Estimates of mean maximum mixing depths in the contiguous United States, Mon. Weather Rev., 92, 235–242, 1964.
Holzworth, G.: Mixing depths, wind speeds and air pollution potential from selected locations in the United States, J. Appl. Met., 6, 1039–1044, 1967.
Kalb, C. P., Dean, A. R., Peppler, R. A., and Sonntag, K. L.: Intercomparison of cloud base height at the ARM Southern Great Plains site, Presented 14th Atmospheric Radiation Measurement (ARM) Science Team Meeting, Albuquerque, NM, US Dept. of Energy, 2004.
Klett, J. D.: Stable analytical inversion solution for processing lidar returns, Appl. Opt., 20, 211–220, 1981.
Lammert, A. and Bosenberg, J.: Determination of the convective boundary layer height with laser remote sensing, Bound.-Layer Meteorol., 119, 159–170, 2006.
Lemonsu, A., Bastin, S., Masson, V., and Drobinski, P.: Vertical structure of the urban boundary layer over Marseille under sea-breeze conditions, Bound.-Layer Meteorol., 118, 477–501, 2006.

ACPD
13, 345–377, 2013

Continuous atmospheric boundary layer in Spain

M. Pandolfi et al.

Martano, P.: An algorithm for the calculation of the time dependent mixing height in coastal site, J. Appl. Meteorol., 41, 351–354, 2002.
Martucci, G., Matthey, C., Mitev, V., and Richner, H.: Comparison between backscatter lidar and radiosonde measurements of the diurnal and nocturnal stratification in the lower troposphere, J. Atmos. Ocean. Technol., 24, 1231–1244, 2007.
Martucci, G., Milroy, C., and O'Dowd, C. D.: Detection of cloud-base height using Jenoptik CHM15K and Vaisala CL31 ceilometers, J. Atmos. Ocean. Technol., 2, 305–318, 2010.
Mastrantonio, G., Viola, A. P., Argentini, S., Fiocco, G., Giannini, L., Rossini, L., Abbate, G., Ocone, R., and Casonato, M.: Observations of sea breeze events in Rome and the surrounding area by a network of Doppler sodars, Bound.-Layer Meteorol., 71, 67–80, 1994.
Matthias, V. and Bösenberg, J.: Aerosol climatology for the planetary boundary layer derived from regular lidar measurements, Atmos. Res., 63, 221–245, 2002.
Matthias, V., Balis, D., Bösenberg, J., Eixmann, R., Iarlori, M., Komguem, L., Mattis, I., Papayannis, A., Pappalardo, G., Perrone, M. R., and Wang, X.: Vertical aerosol distribution over Europe: statistical analysis of Raman lidar data from 10 European Aerosol Research Lidar Network (EARLINET) stations, J. Geophys. Res., 109, D18201, doi:10.1029/2004JD004638, 2004.
Menut, L., Flamant, C., Pelo, J., and Flamant, P. H.: Urban boundary-layer height determination from lidar measurements over Paris area, Appl. Opt., 38, 945–954, 1999.
Millán, M. M., Salvador R., Mantilla E., and Kallos, G.: Photooxidant dynamics in the Mediterranean basin in summer: results from European research projects, J. Geophys. Res., 102, 8811–8823, 1997.
Millán, M. M., Mantilla, E., Salvador, R., Carratalá, A., Sanz, M. J., Alonso, L., Gangoiti, G., and Navazo, M.: Ozone cycles in the western Mediterranean basin: interpretation of monitoring data in complex coastal terrain, J. Appl. Meteorol., 39, 73–83, 2000.
Milroy, C., Martucci, G., Lolli, S., Loaec, S., Sauvage, L., Xueref-Remy, I., Lavrič, J. V., Ciais, P., and O'Dowd, C. D.: On the ability of pseudo-operational ground-based light detection and ranging (LIDAR) sensors to determine boundary-layer structure: intercomparison and comparison with in-situ radiosounding, Atmos. Meas. Tech. Discuss., 4, 563–597, doi:10.5194/amtd-4-563-2011, 2011.
Monks, P., Granier, C., Fuzzi, S., Stohl, A., Williams, M. L., Akimoto, H., Amann, M., Baklanov, A., Baltensperger, U., Bey, I., Blake, N., Blake, R. S., Carslaw, K. S., Cooper, O. R., Dentener, F., Fowler, D., Fragkou, E., Frost, G. J., Generoso, S., Ginoux, P., Grewe, V., Guenther,

ACPD
13, 345–377, 2013

A., Hansson, H. C., Henne, S., Hjorth, J., Hofzumahaus, A., Huntrieser, H., Isaksen, I. S. A., Jenkin, M. E., Kaiser, J., Kanakidou, M., Klimont, Z., Kulmala, M., Laj, P., Lawrence, M., Lee, J. D., Liousse, C., Maione, M., McFiggans, G., Metzger, A., Mieville, A., Moussiopoulos, N., Orlando, J. J., O'Dowd, C. D., Palmer, P. I., Parrish, D. D., Petzold, A., Platt, U., Pöschl, U., Prevot, A. S. H., Reeves, C. E., Reimann, S., Rudich, Y., Sellegri, K., Steinbrecher, R., Simpson, D., ten Brink, H., Theloke, J., van der Werf, G. R., Vautard, R., Vestreng, V., Vlachokostas, Ch., and von Glasow R.: Atmospheric composition change: global and regional air quality, Atmos. Environ., 43, 5268–5350, 2009.

Pandolfi, M., Cusack, M., Alastuey, A., and Querol, X.: Variability of aerosol optical properties in the Western Mediterranean Basin, Atmos. Chem. Phys., 11, 8189–8203, doi:10.5194/acp-11-8189-2011, 2011.

Pappalardo, G., Amodeo, A., Pandolfi, M., Wandinger, U., Ansmann, A., Bosenberg, J., Matthias, V., Amiridis, V., Tomasi, F. D., Frioud, M., Iarlori, M., Komguem, L., Papayannis, A., Rocadenbosch, F., and Wang, X.: Aerosol lidar intercomparison in the framework of the EARLINET Project. 3. Raman lidar algorithm for aerosol extinction, backscatter, and lidar ratio, Appl. Opt., 43, 5370–5385, 2004.

Pay, M. T., Jiménez-Guerrero, P., Jorba, O., Basart, S., Querol, X., Pandolfi, M., and Baldasano, J. M.: Spatio-temporal variability of concentrations and speciation of particulate matter across Spain in the CALIOPE modeling system, Atmos. Environ., 46, 376–396, 2012.

Pérez, C., Sicard, M., Jorba, O., Comerón, A., and Baldasano, J. M.: Summertime recirculations of air pollutants over the north-eastern Iberian coast observed from systematic EARLINET lidar measurements in Barcelona, Atmos. Environ., 38, 3983–4000, 2004.

Pey, J., Alastuey, A., Querol, X., and Rodríguez, S.: Monitoring of sources and atmospheric processes controlling air quality in an urban Mediterranean environment original research article, Atmos. Environ., 44, 4879–4890, 2010.

Querol, X., Alastuey, A., Moreno, T., Viana, M. M., Castillo, S., Pey, J., Rodríguez, S., Artiñano, B., Salvador, P., Sánchez, M., Garcia Dos Santos, S., Herce Garraleta, M. D., Fernandez-Patier, R., Moreno-Grau, S., Negral, L., Minguillón, M. C., Monfort, E., Sanz, M. J., Palomo-Marín, R., Pinilla-Gil, E., Cuevas, E., de la Rosa, J., and Sánchez de la Campa, A.: Spatial and temporal variations in airborne particulate matter (PM_{10} and $PM_{2.5}$) across Spain 1999–2005, Atmos. Environ., 42, 3964–3979, 2008.

Reche, C., Viana, M., Moreno, T., Querol, X., Alastuey, A., Pey, J., Pandolfi, M., Prévôt, A., Mohr, C., Richard, A., Artiñano, B., Gomez-Moreno, F. J., and Cots, N.: Peculiarities in at-

mospheric particle number and size-resolved speciation in an urban area in the western Mediterranean: results from the DAURE campaign, Atmos. Environ., 45, 5282–5293, 2011.
Rodrìguez, S., Querol, X., Alastuey, A., Kallos, G., and Kakaliagou O.: Saharan dust contributions to PM_{10} and TSP levels in Southern and Eastern Spain, Atmos. Environ., 35, 2433–2447, 2001.
Schuster, G. L., Dubovik, O., and Holben, B. N.: Ångström exponent and bimodal aerosol size distributions, J. Geophys. Res., 111, D07207, doi:10.1029/2005JD006328, 2006.
Sicard, M., Pérez, C., Rocadenbosch, F., Baldasano, J. M., and García-Vizcaino, D.: Mixed-layer depth determination in the Barcelona coastal area from regular lidar measurements: methods, results and limitations, Bound.-Lay. Meteorol., 119, 135–157, 2006.
Sicard, M., Rocadenbosch, F., Reba, M. N. M., Comerón, A., Tomás, S., García-Vízcaino, D., Batet, O., Barrios, R., Kumar, D., and Baldasano, J. M.: Seasonal variability of aerosol optical properties observed by means of a Raman lidar at an EARLINET site over Northeastern Spain, Atmos. Chem. Phys., 11, 175–190, doi:10.5194/acp-11-175-2011, 2011.
Stull, R. B.: Introduction to Boundary Layer Meteorology, Kluwer Academic Publisher, Dordrecht, 670 pp., 1998.
Talbot, C., Augustin, P., Leroy, C., Willart, V., Delbarre, H., Khomenco, G.: Impact of a sea breeze on the boundary-layer dynamics and the atmospheric stratification in a coastal area of the North Sea, Bound.-Layer Meteorol., 125, 133–154, 2007.
Tsaknakis, G., Papayannis, A., Kokkalis, P., Amiridis, V., Kambezidis, H. D., Mamouri, R. E., Georgoussis, G., and Avdikos, G.: Inter-comparison of lidar and ceilometer retrievals for aerosol and Planetary Boundary Layer profiling over Athens, Greece, Atmos. Meas. Tech., 4, 1261–1273, doi:10.5194/amt-4-1261-2011, 2011.

ACPD
13, 345–377, 2013

Table 1. Characteristics of measurements and variables presented in this work for the whole SAPUSS campaign (ALL) and for each scenario identified during SAPUSS, namely: African, Atlantic, and Regional. Mean values highlighted in bold (grey cell) indicate the variables for which a significant difference was observed among the three different scenarios.

		SML [m]	DRCL [m]	β_{500} [$\mathrm{M\,m^{-1}\,sr^{-1}}$]	β_{800} [$\mathrm{M\,m^{-1}\,sr^{-1}}$]	PM_1 [$\mathrm{\mu g\,m^{-3}}$]	T [°C]	RH [%]	AOD (**)	Angst. (*)
ALL	mean	**904**	**1761**	**0.59**	**0.87**	**12.6**	**18.5**	**64**	**0.08**	**1.2**
	SD	273	363	0.45	0.68	4.4	3.8	15	0.10	0.4
	median	866	1798	0.45	0.68	10.9	18.6	66	0.05	1.4
	min	430	829	0.06	0.05	7.7	9.3	29	0.01	0.1
	max	1916	2515	3.42	4.78	26.5	26.0	94	0.48	1.7
Atlantic	mean	**965**	**1878**	**0.51**	**0.78**	**9.8**	**17.6**	**55**	**0.03**	**1.3**
	SD	222	290	0.44	0.72	1.1	3.5	13	0.02	0.3
	median	905	1871	0.37	0.55	9.7	17.7	55	0.03	1.3
	min	497	1130	0.09	0.11	8.1	9.3	32	0.01	0.4
	max	1673	2412	2.10	3.55	13.4	24.6	81	0.10	1.7
Regional	mean	**911**	**1769**	**0.64**	**1.01**	**16.3**	**18.5**	**66**	**0.07**	**1.5**
	SD	234	314	0.39	0.64	5.3	3.7	14	0.05	0.2
	median	884	1729	0.59	0.90	14.4	18.3	68	0.05	1.5
	min	483	1282	0.11	0.05	8.6	11.2	29	0.02	0.7
	max	1610	2515	3.42	4.78	26.5	24.9	88	0.25	1.7
African	mean	**736**	**1573**	**0.77**	**1.14**	**11.6**	**21.5**	**75**	**0.24**	**0.7**
	SD	183	428	0.57	0.72	1.6	2.5	10	0.17	0.6
	median	695	1568	0.62	0.81	11.5	21.7	76	0.16	0.8
	min	444	849	0.11	0.08	8.7	16.5	60	0.05	0.1
	max	1261	2387	2.50	3.15	15.5	26.0	94	0.48	1.6

* Calculated between 400 nm and 870 nm; ** AOD at 1020 nm.

ACPD
13, 345–377, 2013

Continuous atmospheric boundary layer in Spain

M. Pandolfi et al.

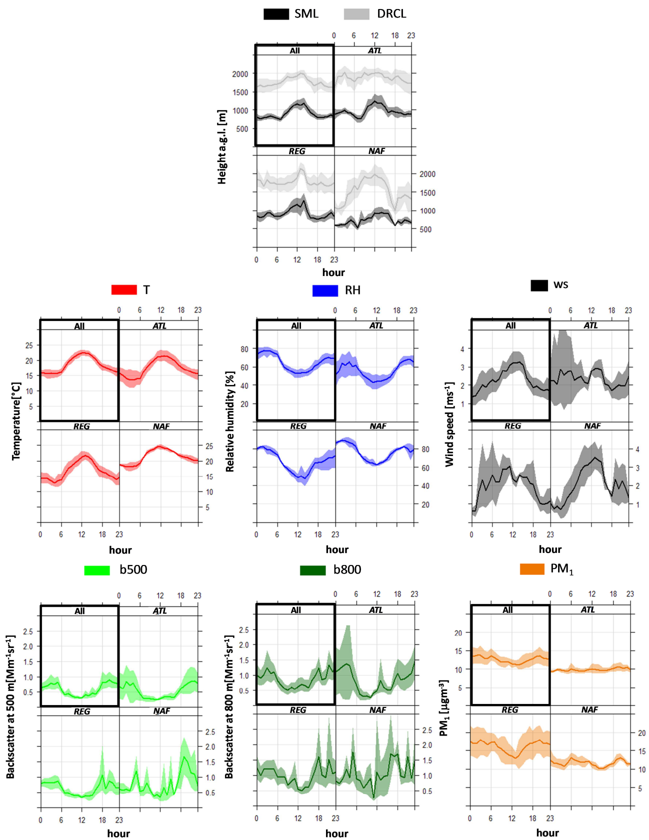

Fig. 1. Diurnal cycles of SML [m], DRCL [m], aerosol backscatter coefficients at 500 m (β_{500}) and 800 m a.g.l. (β_{800}) [$\mathrm{M\,m^{-1}\,sr^{-1}}$], ground temperature ($T$) [°C], relative humidity (RH) [%], wind speed [$\mathrm{m\,s^{-1}}$], and PM_1 concentrations [$\mathrm{\mu g\,m^{-3}}$] calculated for the entire SAPUSS campaign (All) and for the ATL, REG, and NAF scenarios.

ACPD
13, 345–377, 2013

Title Page
Abstract | Introduction
Conclusions | References
Tables | Figures
◀ | ▶
Back | Close
Full Screen / Esc
Printer-friendly Version
Interactive Discussion

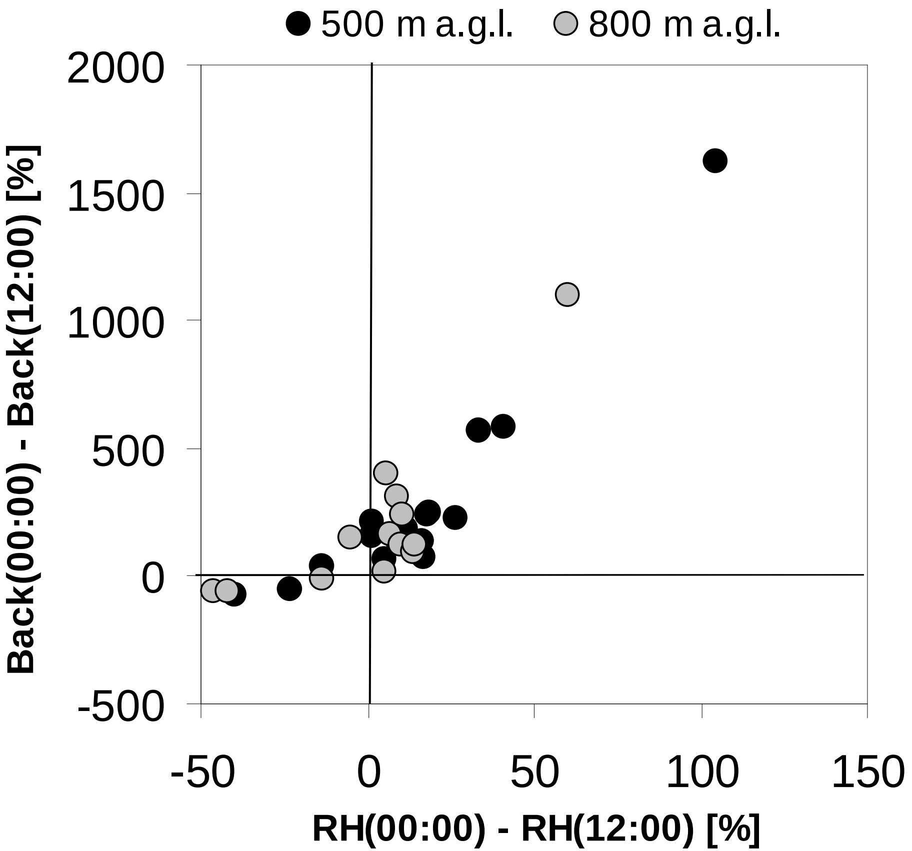

Fig. 2. Relationship between the relative variations [%] in relative humidity (RH) and aerosol backscatter coefficients between night (00:00 UTC) and day (12:00 UTC) at 500 m a.g.l. and 800 m a.g.l.

ACPD
13, 345–377, 2013

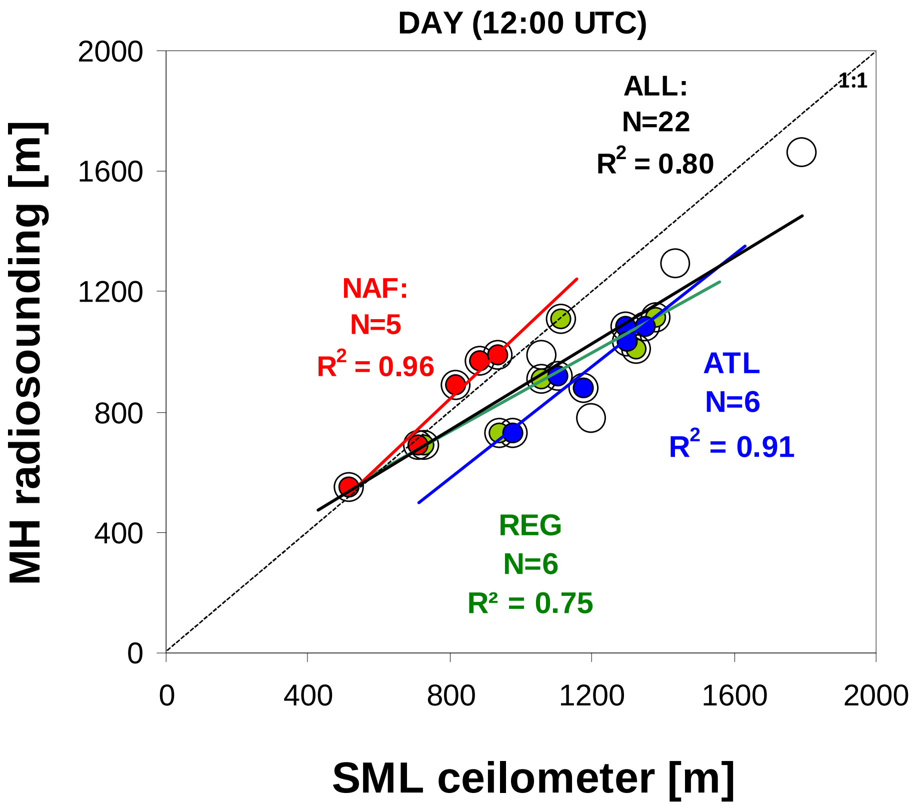

Fig. 3. Correlation between SML heights retrieved from ceilometer and radiosoundings at 12:00 UTC for the whole SAPUSS campaign (open circles) and separately for the Regional (REG; green circles), African (NAF; red circles), and Atlantic (ATL; blue circles) scenarios. N: number of aerosol backscatter and potential temperature vertical profiles pairs; R^2: coefficient of determination.

ACPD
13, 345–377, 2013

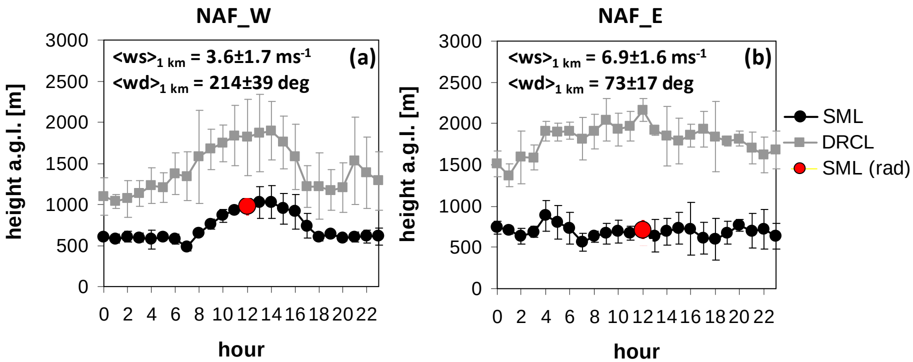

Fig. 4. Mean SML (black dotted line) and DRCL (grey dotted line) diurnal cycles from ceilometer and SML heights from radiosoundings retrieved at 12:00 GMT (red dot) averaged during the NAF_W days **(a)** and the NAF_E days **(b)**. Error bars represent one standard deviation of the means. $\langle ws \rangle_{1\,km}$ and $\langle wd \rangle_{1\,km}$ stand for mean wind speed and direction, respectively, averaged within the first kilometre of height from radiosoundings.

ACPD
13, 345–377, 2013

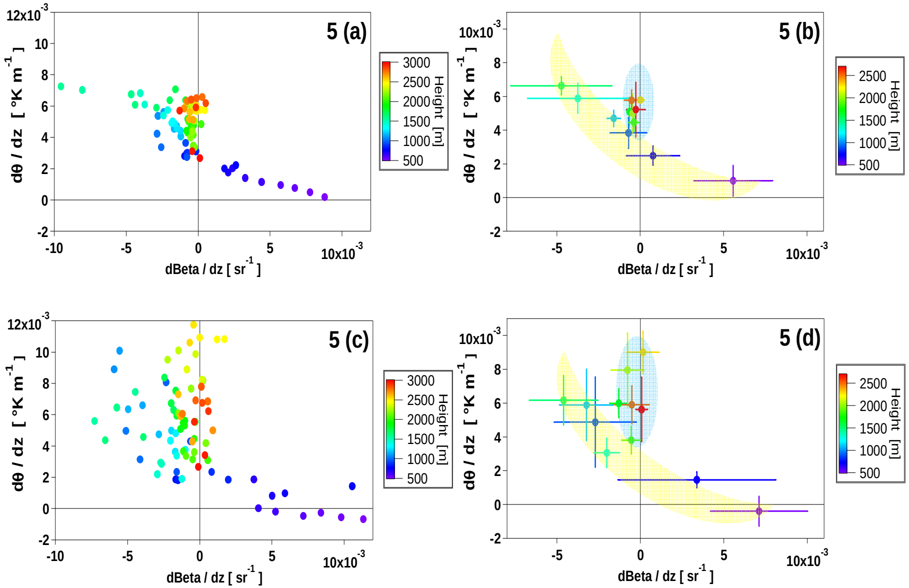

Fig. 5. Relationship between the first derivatives as a function of the height of aerosol backscatter (Beta) and potential temperature (θ) vertical profiles: **(a)** by using the points from 500 m to 3000 m a.g.l. (30 m vertical resolution) of one pair of beta and θ vertical profiles obtained by averaging 14 available profile pairs; **(b)** by averaging the points of **(a)** every 200 m with the error bars indicating ±1 standard deviation of the means; **(c)** by using the points from 500 m to 3000 m a.g.l. (30 m vertical resolution) of one pair of beta and θ vertical profiles obtained by averaging a subset of 4 profile pairs; **(d)** by averaging the points of **(c)** every 200 m with the error bars indicating ±1 standard deviation of the means. Yellow and blue coloured areas in **(b)** and **(d)** indicate the SML+DRCL and the free troposphere, respectively.

ACPD
13, 345–377, 2013

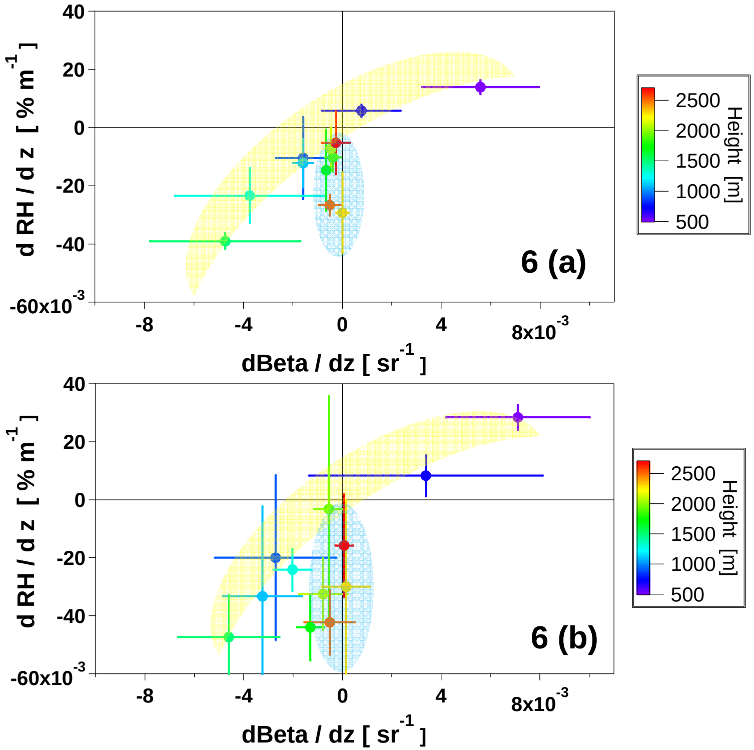

Fig. 6. Relationship between the first derivatives as a function of the height of aerosol backscatter (Beta) and relative humidity (RH) vertical profiles: **(a)** by using the points from 500 m to 3000 m a.g.l. (averaged every 200 m) of one pair of Beta and RH vertical profiles obtained by averaging 14 available profile pairs; **(b)** by using the points from 500 m to 3000 m a.g.l. (averaged every 200 m) of one pair of Beta and RH vertical profiles obtained by averaging a subset of 4 profile pairs. Error bars indicate ±1 standard deviation of the means. Yellow and blue coloured areas indicate the SML+DRCL and the free troposphere, respectively.

ACPD
13, 345–377, 2013

Continuous atmospheric boundary layer in Spain

M. Pandolfi et al.